Doppler-free laser spectroscopy

8

Doppler broadening is usually the dominant contribution to the observed width of lines in atomic spectra, at room temperature. The techniques of Doppler-free laser spectroscopy overcome this limitation to give much higher resolution than, for example, a Fabry–Perot étalon analyzing the light from a discharge lamp, as shown in Fig. 1.7(a). This chapter describes three examples that illustrate the principles of Doppler-free techniques: the crossed-beam method, saturated absorption spectroscopy and two-photon spectroscopy. To use these high resolution techniques for precision measurements of atomic transition frequencies the laser frequency must be determined accurately. Thus the calibration is a crucial part of laser spectroscopy experiments, as discussed at the end of this chapter. Since it is important to understand the problem before looking at the solution, the chapter starts with an outline of Doppler broadening of spectral lines in gases.

8.1 Doppler broadening of spectral lines

The relationship between the angular frequency ω of radiation in the laboratory frame of reference and the angular frequency seen in a frame of reference moving at velocity $\mathbf{v}$, as shown in Fig. 8.1, is

$$\omega' = \omega - kv\,, \tag{8.1}$$

where the wavevector of the radiation has magnitude $k = \omega/c = 2\pi/\lambda$. It is the component of the velocity along $\mathbf{k}$ that leads to the Doppler effect and here it has been assumed that $\mathbf{k}\cdot\mathbf{v} = kv$.[1]

[1] If necessary, this and other equations in this chapter could be generalised by replacing kv with the scalar product $\mathbf{k}\cdot\mathbf{v}$.

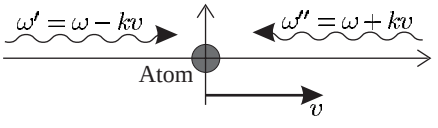

Fig. 8.1 The Doppler effect on the observed frequency of radiation. Radiation that has an angular frequency of ω in the laboratory frame of reference has the frequencies indicated in a reference frame moving with a speed v, e.g. the rest frame of an atom. Only the component of the velocity along the wavevector $\mathbf{k}$ contributes to the first-order Doppler shift.

In this section, we consider the Doppler effect on the absorption by a gas where each atom absorbs radiation at frequency ω_0 in its rest frame, i.e. when $\omega' = \omega_0$.[2] Thus atoms moving with velocity v absorb radiation when $\delta = \omega - \omega_0 = kv$, or equivalently

$$\frac{\delta}{\omega_0} = \frac{v}{c}\,. \tag{8.2}$$

In a gas the fraction of atoms with velocity in the range v to $v + \mathrm{d}v$ is

$$f(v)\,\mathrm{d}v = \sqrt{\frac{M}{\pi 2k_\mathrm{B}T}}\,\exp\left(-\frac{Mv^2}{2k_\mathrm{B}T}\right)\mathrm{d}v \equiv \frac{1}{u\sqrt{\pi}}\,\exp\left(-\frac{v^2}{u^2}\right)\mathrm{d}v\,. \tag{8.3}$$

Here $u = \sqrt{2k_\mathrm{B}T/M}$ is the most probable speed for atoms of mass M at temperature T.[3] Relating v to the frequency via eqn 8.2, we find that the absorption has the Gaussian line shape function[4]

$$g_\mathrm{D}(\omega) = \frac{c}{u\omega_0\sqrt{\pi}}\exp\left\{-\frac{c^2}{u^2}\left(\frac{\omega-\omega_0}{\omega_0}\right)^2\right\}. \tag{8.4}$$

The maximum value occurs at $\omega = \omega_0$ and the function falls to half its maximum value at $\omega - \omega_0 = \delta_{1/2}$, where

$$\left(\frac{c\,\delta_{1/2}}{u\,\omega_0}\right)^2 = \ln 2\,. \tag{8.5}$$

The Doppler-broadened line has a full width at half maximum (FWHM) of $\Delta\omega_\mathrm{D} = 2\delta_{1/2}$ given by[5]

$$\frac{\Delta\omega_\mathrm{D}}{\omega_0} = 2\sqrt{\ln 2}\,\frac{u}{c} \simeq 1.7\,\frac{u}{c}\,. \tag{8.6}$$

Kinetic theory gives the most probable speed in a gas as

$$u = 2230\,\mathrm{m\,s^{-1}} \times \sqrt{\frac{T}{300\,\mathrm{K}} \times \frac{1\,\mathrm{a.m.u.}}{M}}\,. \tag{8.7}$$

[2] Section 8.3 describes what happens when the atoms absorb a range of frequencies, given by the homogeneous width, in addition to any Doppler broadening. Absorption is considered here because of its relevance to laser spectroscopy, but Doppler broadening of an emission line arises in the same way—atoms emit at ω_0 in their rest frame and we see a frequency shift in the laboratory.

[3] This can easily be shown by differentiating the Maxwell speed distribution which is proportional to v^2 times the velocity distribution, see Table 8.1.

[4] Note that $\int_{-\infty}^{\infty} g(\omega)\,\mathrm{d}\omega = 1$.

[5] The simple estimate of the FWHM as $\sim 2u/c$ that leads to eqn 6.38 turns out to be quite accurate.

Table 8.1 The characteristic velocities in a gas with a Maxwellian distribution of speeds and in an effusive atomic beam; $u = \sqrt{2k_\mathrm{B}T/M}$, where T is the temperature and M is the mass. The extra factor of v in the distribution for a beam, as compared to that of a gas, arises from the way that atoms effuse through a small hole of area A. Atoms with speed v are incident on a surface of area A at a rate of $N(v)\,vA/4$, where $N(v)$ is the number density of atoms with speeds in the range v to $v + \mathrm{d}v$—faster atoms are more likely to pass through the hole. Integration over v leads to the well-known kinetic theory result $N\overline{v}A/4$ for the flux that arrives at the surface, where N is the total number density. The mean speed $\overline{v}$ has a value between the most probable and the root-mean-square velocities.

	Gas	Beam
Distribution	$v^2\exp\left(-v^2/u^2\right)$	$v^3\exp\left(-v^2/u^2\right)$
Most probable v	u	$\sqrt{3/2}\,u$
Root-mean-square velocity	$\sqrt{3/2}\,u$	$\sqrt{2}\,u$

In the formula, the atomic mass M must be expressed in atom mass units, e.g. $M = 1$ a.m.u. for atomic hydrogen. Numerical values of u are given below for hydrogen and a vapour of caesium, both at a temperature of $T = 300\,\mathrm{K}$.[6]

[6] In this table $\Delta f_\mathrm{D} = 1.7u/\lambda$.

	M (a.m.u.)	$u\,(\mathrm{m\,s^{-1}})$	$\Delta\omega_\mathrm{D}/\omega_0$	Δf_D (GHz), for 600 nm
H	1	2230	1×10^{-5}	6
Cs	133	200	1×10^{-6}	0.5

The values given for the fractional width $\Delta\omega_\mathrm{D}/\omega_0$ show that heavy elements have an order of magnitude smaller Doppler width than hydrogen. The Doppler shift of the frequency Δf_D is also given for a wavelength of 600 nm. (This wavelength does not correspond to actual transitions.[7]) These calculations show that Doppler broadening limits optical spectroscopy to a resolution of $\sim 10^6$ even for heavy elements.[8]

The Doppler effect on the absorption of a gas is an example of an inhomogeneous broadening mechanism; each atom interacts with the radiation in a different way because the frequency detuning, and hence absorption and emission, depend on the velocity of the individual atom. In contrast, the radiative broadening by spontaneous decay of the excited level gives the same natural width for all atoms of the same species in a gas—this is a homogeneous broadening mechanism.[9] The difference between homogeneous and inhomogeneous broadening is crucially important in laser physics and an extensive discussion and further examples can be found in Davis (1996) and Corney (2000).[10]

[7] The Doppler widths of optical transitions in other elements normally lie between the values for H and Cs. A useful way to remember the correct order of magnitude is as follows. The speed of sound in air is $330\,\mathrm{m\,s^{-1}}$ (at $0\,^\circ$C), slightly less than the speed of the air molecules. The speed of sound divided by the speed of light equals 10^{-6}. Multiplication by a factor of 2 converts the half-width to a FWHM of $\Delta\omega_\mathrm{D}/\omega_0 \simeq 2 \times 10^{-6}$, which gives a reasonable estimate of the fractional Doppler shift of medium-heavy elements.

[8] The resolving power of a Fabry–Perot étalon can easily exceed $\sim 10^6$ (Brooker 2003), so that normally the instrumental width does not limit the resolution, in the visible region.

[9] The different characteristics of the two types of broadening mechanism are discussed further in this chapter, e.g. see Fig. 8.3.

[10] The treatment of the saturation of gain in different classes of laser system is closely related to the discussion of saturation of absorption, both in principle and also in the historical development of these subjects.

8.2 The crossed-beam method

Figure 8.2 shows a simple way to reduce the Doppler effect on a transition. The laser beam intersects the atomic beam at right angles. A thin vertical slit collimates the atomic beam to give a small angular spread α. This gives a spread in the component of the atomic velocity along the direction of the light of approximately αv_beam. Atoms in the beam have slightly higher characteristic velocities than in a gas at the same temperature, as shown in Table 8.1, because faster atoms have a higher probability of effusing out of the oven. Collimation reduces the Doppler broadening to

$$\Delta f \simeq \frac{\alpha v_\mathrm{beam}}{\lambda} \sim \alpha \Delta f_\mathrm{D}\,, \tag{8.8}$$

where Δf_D is the Doppler width of a gas at the same temperature as the beam.[11]

[11] A numerical factor of $0.7 \simeq 1.2/1.7$ has been dropped. To obtain a precise formula we would have to consider the velocity distribution in the beam and its collimation—usually the exit slit of the oven and the collimation slit have comparable widths.

Example 8.1 *Calculation of the collimation angle for a beam of sodium that gives a residual Doppler broadening comparable with the natural width $\Delta f_\mathrm{N} = 10\,MHz$ (for the resonance transition at $\lambda = 589\,nm$)*

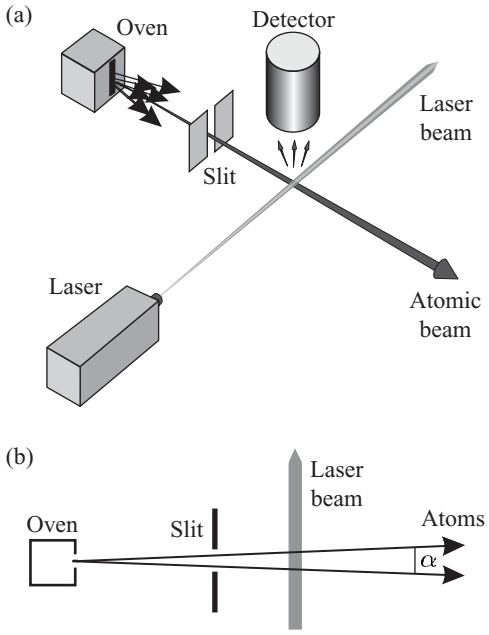

Fig. 8.2 Laser spectroscopy of a collimated atomic beam. The component of atomic velocity along the laser beam has a small spread $\alpha v_{\rm beam}$, where α is the collimation angle shown on the plan view in (b).

Sodium vapour at 1000 K has a Doppler width of $\Delta f_{\rm D} = 2.5\,{\rm GHz}$ and the most probably velocity in the beam is $v_{\rm beam} \simeq 1000\,{\rm m\,s^{-1}}$. Thus a suitable collimation angle for a beam of sodium effusing from an oven at this temperature is

$$\alpha = \frac{\Delta f_{\rm N}}{\Delta f_{\rm D}} = \frac{10}{2500} = 4 \times 10^{-3}\,{\rm rad}\,. \tag{8.9}$$

This angle corresponds to a slit 1 mm wide positioned 0.25 m from the oven. Collimation of the beam to a smaller angular spread would just throw away more of the atomic flux to give a weaker signal without reducing the observed line width.

In this experiment, atoms interact with the light for a time $\Delta t \simeq d/v_{\rm beam}$, where d is the laser beam diameter. The finite interaction time leads to a spread in frequencies called transit-time broadening.[12] For a laser beam of diameter 1 mm we find

$$\Delta f_{\rm tt} = \frac{v_{\rm beam}}{d} = \frac{1000}{10^{-3}} \simeq 1\,{\rm MHz}\,. \tag{8.10}$$

Thus this broadening mechanism does not have a significant effect in this experiment, compared to the natural width of the optical transition. (Transit time is an important consideration for the radio-frequency measurements with atomic beams described in Section 6.4.2.) Collision broadening has a negligible effect in the experiment shown in Fig 8.2 because of the low density of atoms in the atomic beam and also in the background gas in the vacuum chamber. An atomic-beam apparatus must have a high vacuum since even a glancing collision with a

[12] From eqn 7.50, $\Delta f \simeq 1/\Delta t$.

background gas molecule deflects an atom out of the highly-collimated beam.

Example 8.2 Figure 6.12 in the chapter on hyperfine structure showed a spectrum of tin (Sn) obtained by the crossed-beam technique that illustrated isotope and hyperfine structure. Comparison with the Doppler-broadened spectrum emitted by a cadmium lamp clearly showed the advantages of the crossed-beam technique.[13]

[13] The spacings between the lines from different isotopes does not depend on the angle between the laser beam and the atomic beam, but for absolute measurements of transition frequencies the angle must be accurately set to 90°.

Experimenters used highly-monochromatic light sources to demonstrate the principle of the crossed-beam method before the advent of lasers, but the two other techniques described in this chapter rely on the high-intensity and narrow-frequency bandwidth of laser light.

8.3 Saturated absorption spectroscopy

We derived the line shape for Doppler broadening in Section 8.1 on the assumption that an atom at rest absorbs radiation exactly at ω_0. In reality the atoms absorb radiation over a range of frequencies given by the homogeneous width of the transition, e.g. the line width Γ caused by radiative broadening. In this section we shall reconsider absorption of monochromatic radiation in a way that includes homogeneous broadening together with the inhomogeneous broadening caused by the atom's motion. This approach leads naturally into a discussion of saturated absorption spectroscopy.

We consider a laser beam of intensity $I(\omega)$ that travels through a sample of atoms, as shown in Fig. 7.4. In this chapter we consider the atoms as moving, whereas previously they were taken to be stationary.[14] Atoms with velocities in the velocity class v to $v + \mathrm{d}v$ see radiation with an effective frequency of $\omega - kv$ in their rest frame, and for those atoms the absorption cross-section is $\sigma(\omega - kv)$, defined in eqn 7.76. The number density of atoms in this velocity class is $N(v) = Nf(v)$, where N is the total number density of the gas (in units of atoms m^{-3}) and the distribution $f(v)$ is given in eqn 8.3. Integration of the contributions from all the velocity classes gives the absorption coefficient as

[14] At room temperature, the Doppler width usually exceeds natural and other homogeneous broadening mechanisms. Very cold atomic vapours in which the Doppler shifts are smaller than the natural width of allowed transitions can be prepared by the laser cooling techniques described in Chapter 9.

$$\begin{aligned}\kappa(\omega) &= \int N(v)\,\sigma(\omega - kv)\,\mathrm{d}v \\ &= \frac{g_2}{g_1}\,\frac{\pi^2 c^2}{\omega_0^2} A_{21} \times \int N(v)\, g_{\mathrm{H}}(\omega - kv)\,\mathrm{d}v \qquad (8.11) \\ &= \frac{g_2}{g_1}\,\frac{\pi^2 c^2}{\omega_0^2} A_{21} \times N \int f(v)\,\frac{\Gamma/(2\pi)}{(\omega - \omega_0 - kv)^2 + \Gamma^2/4}\,\mathrm{d}v\,.\end{aligned}$$

The integral is the convolution of the Lorentzian function $g_{\mathrm{H}}(\omega - kv)$ and the Gaussian function $f(v)$.[15] Except at very low temperatures the homogenous width is much less than the Doppler broadening, $\Gamma \ll \Delta\omega_{\mathrm{D}}$, so that the Lorentzian is sharply peaked and acts like a delta function

[15] In general, the convolution leads to a Voigt function that needs to be calculated numerically (Corney 2000 and Loudon 2000).

$g_{\rm H}(\omega - kv) \equiv \delta(\omega - \omega_0 - kv)$ that picks out atoms moving with velocity

$$v = \frac{\omega - \omega_0}{k}\,. \tag{8.12}$$

Integration over v transforms $f(v)$ into the Gaussian line shape function in eqn 8.4:[16]

$$g_{\rm D}(\omega) = \int f(v)\, g_{\rm H}(\omega - kv)\, {\rm d}v\,. \tag{8.13}$$

[16] This is a convolution of the solution for a stationary atom with the velocity distribution (cf. Exercise 7.9).

Thus since $\kappa(\omega) = N\sigma(\omega)$ (from eqn 7.70) we find from eqn 8.11 that the cross-section for Doppler-broadened absorption is

$$\sigma(\omega) = \frac{g_2}{g_1}\frac{\pi^2 c^2}{\omega_0^2} A_{21}\, g_{\rm D}(\omega)\,. \tag{8.14}$$

Integration of $g_{\rm D}(\omega)$ over frequency gives unity, as in eqn 7.78 for homogeneous broadening. Thus both types of broadening have the same integrated cross-section, namely[17]

$$\int_0^\infty \sigma(\omega)\, {\rm d}\omega = \frac{g_2}{g_1}\frac{\lambda_0^2}{4} A_{21}\,. \tag{8.15}$$

[17] The cross-section only has a significant value near ω_0, so taking the lower limit of the integration to be 0 (which is realistic) or $-\infty$ (which is easy to evaluate) makes little difference.

The line broadening mechanisms spread this integrated cross-section out over a range of frequencies so that the peak absorption decreases as the frequency spread increases. The ratio of the peak cross-sections approximately equals the ratio of the line widths:

$$\frac{[\sigma(\omega_0)]_{\rm Doppler}}{[\sigma(\omega_0)]_{\rm Homog}} = \frac{g_{\rm D}(\omega_0)}{g_{\rm H}(\omega_0)} = \sqrt{\pi \ln 2}\frac{\Gamma}{\Delta\omega_{\rm D}}\,. \tag{8.16}$$

The numerical factor $\sqrt{\pi \ln 2} = 1.5$ arises in the comparison of a Gaussian to a Lorentzian. For the 3s–3p resonance line of sodium $\Gamma/2\pi = 10\,{\rm MHz}$ and at room temperature $\Delta\omega_{\rm D}/2\pi = 1600\,{\rm MHz}$, so the ratio of the cross-sections in eqn 8.16 is $\simeq 1/100$. The Doppler-broadened gas gives less absorption, for the same N, because only 1% of the atoms interact with the radiation at the line centre—these are the atoms in the velocity class with $v = 0$ and width $\Delta v \simeq \Gamma/k$. For homogeneous broadening all atoms interact with the light in the same way, by definition.

8.3.1 Principle of saturated absorption spectroscopy

This method of laser spectroscopy exploits the saturation of absorption to give a Doppler-free signal. At high intensities the population difference between two levels is reduced as atoms are excited to the upper level, and we account for this by modifying eqn 8.11 to read

$$\kappa(\omega) = \int_{-\infty}^{\infty} \{N_1(v) - N_2(v)\}\, \sigma_{\rm abs}(\omega - kv)\, {\rm d}v\,. \tag{8.17}$$

This is the same as the modification we made in going from eqn 7.70 to 7.72 but applied to each velocity class within the distribution. Here $N_1(v)$ and $N_2(v)$ are the number densities in levels 1 and 2, respectively, for atoms with velocities between v and $v + \mathrm{d}v$. At low intensities almost all the atoms stay in level 1, so $N_1(v) \simeq N(v)$ has the Gaussian distribution in eqn 8.3 and $N_2 \simeq 0$, as illustrated in Fig. 8.3(a). For all intensities, the integral of the number densities in each velocity class equals the total number density in that level, i.e.

$$\int_{-\infty}^{\infty} N_1(v)\,\mathrm{d}v = N_1\,, \tag{8.18}$$

and similarly for N_2. The total number density $N = N_1 + N_2$.[18]

In saturated absorption spectroscopy the quantity $N_1(v) - N_2(v)$ is affected by interaction with a strong laser beam, as shown in Fig. 8.3(b) and Fig. 8.4 shows a typical experimental arrangement. The beam splitter divides the power of the laser beam between a weak probe and a stronger pump beam.[19] Both these beams have the same frequency ω and the two beams go in opposite directions through the sample cell containing the atomic vapour. The pump beam interacts with atoms that have velocity $v = (\omega - \omega_0)/k$ and excites many of them into the upper level, as shown in Fig. 8.3(b). This is referred to as hole burning. The hole burnt into the lower-level population by a beam of intensity I has a width

$$\Delta\omega_{\mathrm{hole}} = \Gamma\left(1 + \frac{I}{I_{\mathrm{sat}}}\right)^{1/2}\,, \tag{8.19}$$

equal to the power-broadened homogeneous width in eqn 7.88.

When the laser has a frequency far from resonance, $|\omega - \omega_0| \gg \Delta\omega_{\mathrm{hole}}$, the pump and probe beams interact with different atoms so the pump beam does not affect the probe beam, as illustrated on the left- and

[18] This treatment of saturation is restricted to two-level atoms. Real systems with degeneracy are more difficult to treat since, under conditions with signification saturation of the absorption, the atoms are usually not uniformly distributed over the sublevels (unless the light is unpolarized). Nevertheless, the expression $N_1(v) - g_1 N_2(v)/g_2$ is often used for the difference in population densities in a given velocity class.

[19] Normally, we have $I_{\mathrm{probe}} \ll I_{\mathrm{sat}}$ and $I_{\mathrm{pump}} \gtrsim I_{\mathrm{sat}}$.

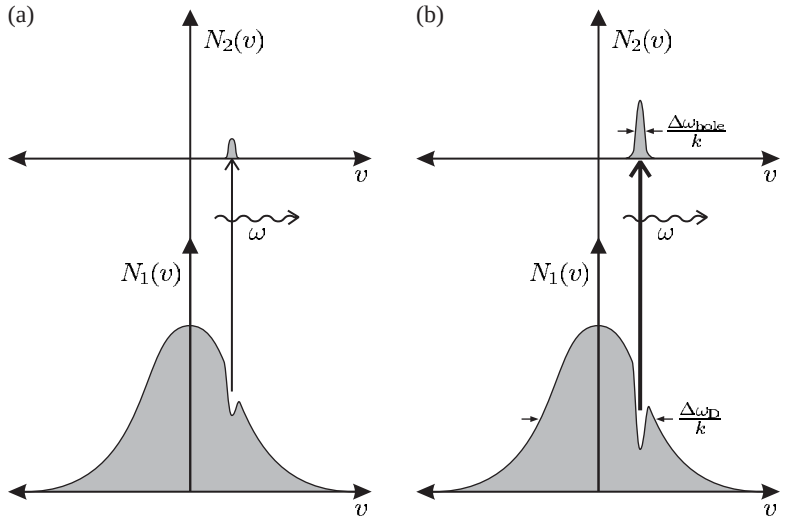

Fig. 8.3 The saturation of absorption. (a) A weak beam does not significantly alter the number density of atoms in each level. The number density in the lower level $N_1(v)$ has a Gaussian distribution of velocities characteristic of Doppler broadening of width $\Delta\omega_{\mathrm{D}}/k$. The upper level has a negligible population, $N_2(v) \simeq 0$. (b) A high-intensity laser beam burns a deep hole—the population difference $N_1(v) - N_2(v)$ tends to zero for the atoms that interact most strongly with the light (those with velocity $v = (\omega - \omega_0)/k$). Note that $N_1(v)$ does *not* tend to zero: strong pumping of a two-level system never gives population inversion. This figure also shows clearly that Doppler broadening is inhomogeneous so that atoms interact in different ways within the radiation.

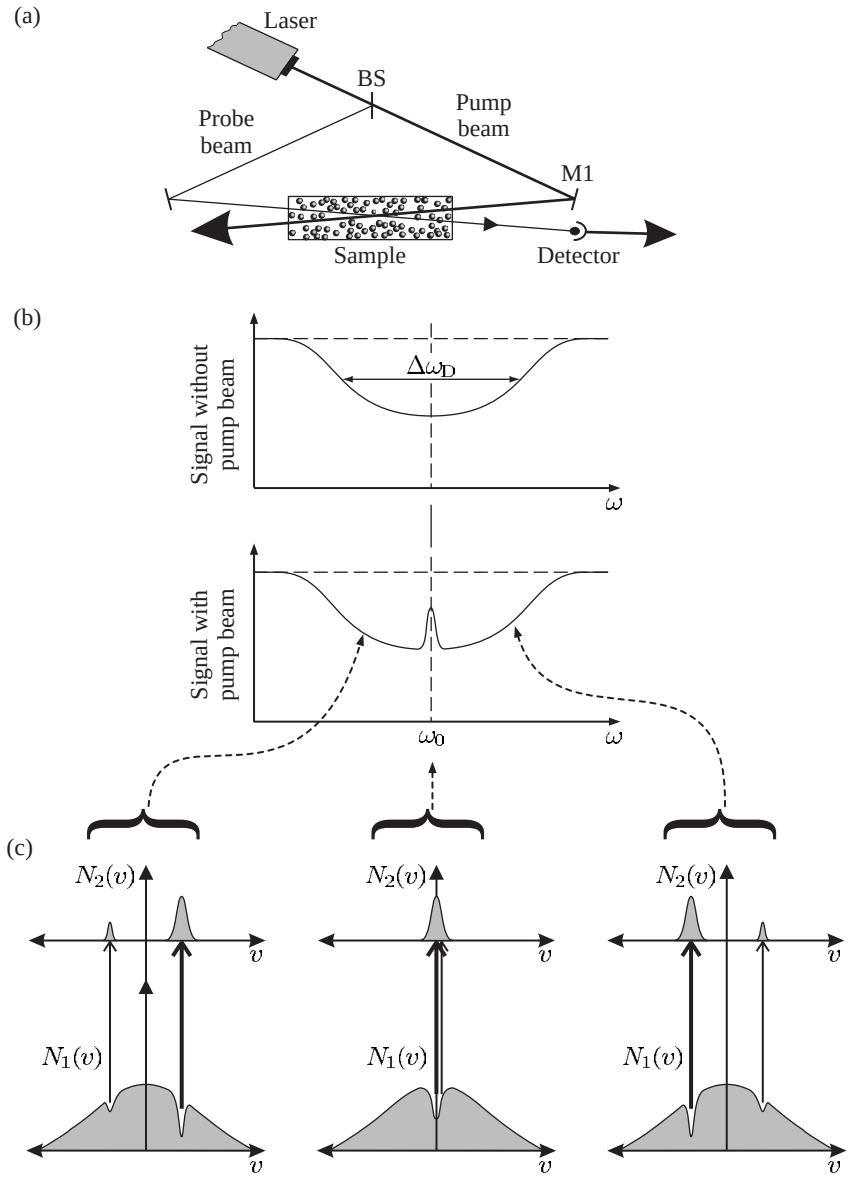

Fig. 8.4 (a) A saturated absorption spectroscopy experiment. The beam splitter BS, e.g. a piece of glass, divides the laser power between a weak probe and a stronger pump beam. The figure shows a finite angle of intersection between the weak probe beam and the stronger pump beam in the sample; this arrangement makes it straightforward to detect the probe beam after the cell but it leaves some residual Doppler broadening. Therefore saturated absorption experiments often have the pump and probe beams exactly counter-propagating and use a partially-reflecting mirror at M1 to transmit some of the probe beam to the detector (while still reflecting enough of the pump beam). (b) A plot of the probe intensity transmitted through the sample as a function of the laser frequency. With the pump beam blocked the experiment gives a simple Doppler-broadened absorption, but in the presence of the pump beam a narrow peak appears at the atomic resonance frequency. (c) The population densities of the two levels $N_1(v)$ and $N_2(v)$ as a function of velocity for three different laser frequencies: below, equal to, and above the atomic resonance, showing the effect of the pump and probe beams.

right-hand sides of Fig. 8.4(c). Close to resonance, $\omega \simeq \omega_0$, both beams interact with atoms in the velocity class with $v \simeq 0$, and the hole burnt by the pump beam reduces the absorption of the probe beam. Thus saturation of the absorption by the pump beam leads to a narrow peak in the intensity of the probe beam transmitted through the sample, as shown in Fig. 8.4(b). Normally, the pump beam has an intensity of about the saturation intensity $I_{\rm sat}$, so the saturated absorption peaks always have a line width greater than the natural width. The *velocity class* of atoms that interact with the light has a velocity spread $\Delta v = \Delta\omega_{\rm hole}/k$.

This section shows how saturation spectroscopy picks out a signal from the atoms in the velocity class centred at $v = 0$ to give a signal at the atomic resonance frequency. It is the homogeneous broadening of these stationary atoms that determines the widths of the peaks. Exercise 8.8 goes through a detailed calculation of this width. Many experiments use this Doppler-free technique to give a stable reference, e.g. to set the laser frequency a few line widths below resonance in laser cooling experiments with the optical molasses technique (described in the next chapter).[20]

[20] Nowadays, inexpensive semiconductor diode lasers make saturation spectroscopy a feasible experiment in undergraduate teaching laboratories, using the alkali elements rubidium or caesium that have sufficient vapour pressure at room temperature that a simple glass cell can be used as the sample (Wieman *et al.* 1999).

8.3.2 Cross-over resonances in saturation spectroscopy

In a saturated absorption spectrum, peaks appear at frequencies midway between pairs of transitions that have energy levels in common (and a separation less than the Doppler width), e.g. for the three-level atom shown in Fig. 8.5(a). To explain these cross-over resonances we need to consider the situation shown in Fig. 8.5(b), where the pump beam burns two holes in the velocity distribution. These holes give rise to two peaks in the spectrum when the laser frequency corresponds to the frequencies of the two transitions—the 'expected' saturated absorption signals for these two transitions. However, an additional peak appears when the hole burnt by one transition reduces the absorption for the other transition. As illustrated by Fig. 8.5(b), the symmetry of this situation means that cross-overs occur exactly midway between two saturated absorption peaks. This property allows experimenters to identify the cross-overs in a saturated absorption spectrum (see the exercises at the end of this chapter), and these extra peaks do not generally cause confusion.

The spectral lines of atomic hydrogen have large Doppler widths because it is the lightest element, but physicists want to measure the energy levels of this simple atom precisely to test atomic physics theory and to determine the Rydberg constant.

Figure 8.6 shows a spectrum of the Balmer-α line ($n = 2$ to $n = 3$) that is limited by Doppler broadening. This red line of atomic hydrogen, at a wavelength of $\lambda = 656\,\text{nm}$, has a Doppler width of $\Delta f_{\rm D} = 6\,\text{GHz}$ at room temperature (Section 8.1); this is less than the 11 GHz interval between the $j = 1/2$ and $3/2$ fine-structure levels in the $n = 2$ shell. Using the isotope deuterium (which has twice the atomic mass of hydrogen) in a discharge cooled to 100 K reduces the Doppler width to $\Delta f_{\rm D} = 2.3\,\text{GHz}$,[21] where one factor arises from the mass and the other from the

[21] As calculated by scaling the value for hydrogen. The ratio of the Doppler widths for H at $T = 300\,\text{K}$ and D at $T = 100\,\text{K}$ is $\sqrt{6} = \sqrt{2} \times \sqrt{3}$.

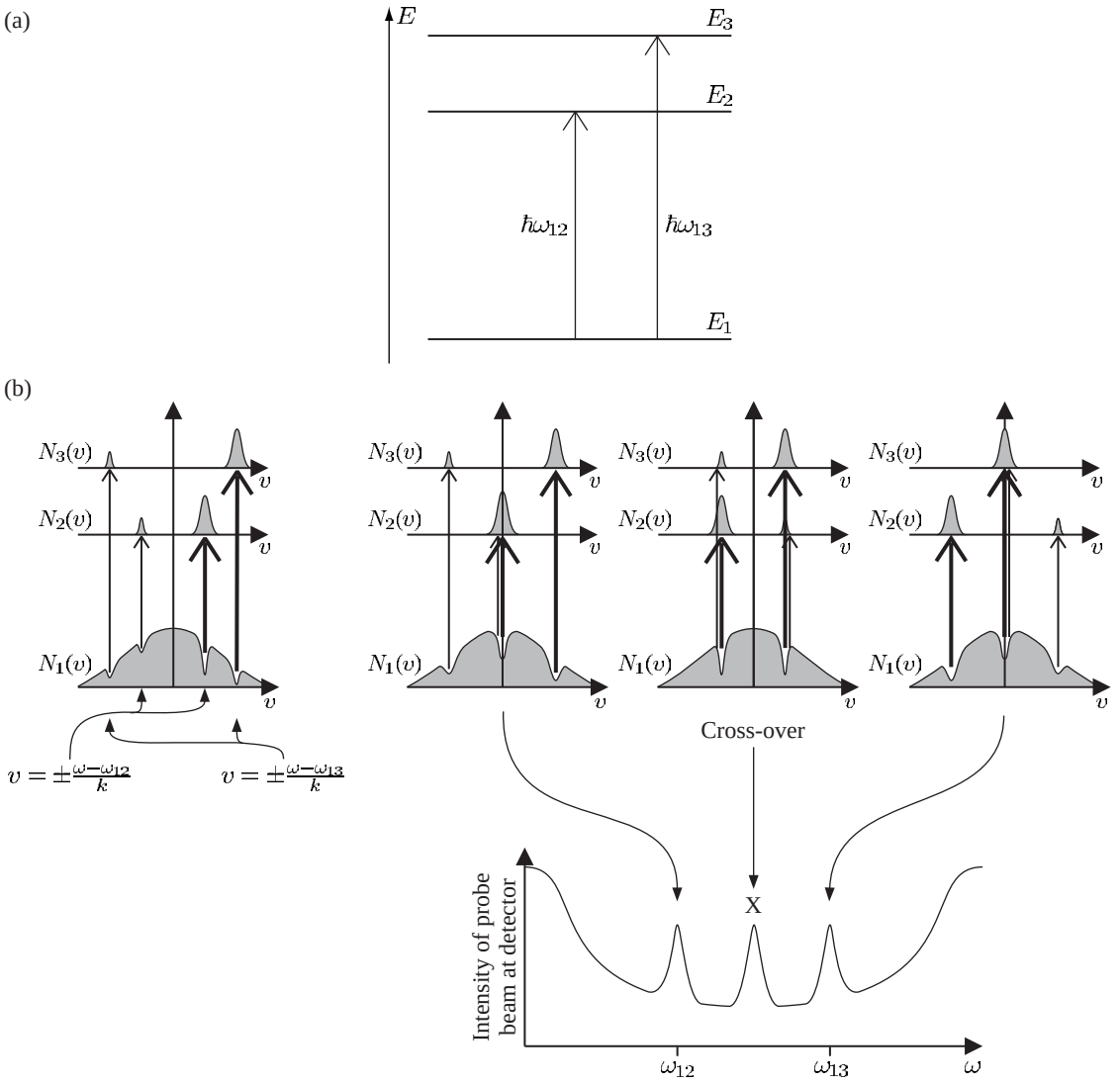

Fig. 8.5 The formation of a cross-over resonance. (a) A three-level atom with two allowed transitions at angular frequencies ω_{12} and ω_{13}. (b) A cross-over resonance occurs at X, midway between two saturated absorption peaks corresponding to transitions at angular frequencies ω_{12} and ω_{13}. At the cross-over the hole burnt by the pump beam acting on transition $1 \leftrightarrow 2$ reduces the probe beam absorption on transition $1 \leftrightarrow 3$, and vice versa.

temperature. This makes it possible to observe components separated by the 3.3 GHz interval between the $j = 1/2$ and $3/2$ fine-structure levels in the $n = 3$ shell—see Figs 8.6(c) and 8.7(a).[22] Structure on the scale of the 1 GHz corresponding to the Lamb shift cannot be resolved by conventional Doppler-limited techniques.

Figure 8.7 shows the spectacular improvement in resolution obtained with Doppler-free spectroscopy. The saturated absorption spectrum shown in Fig. 8.7(c) was obtained in a room-temperature discharge of

[22] The expectation value of the spin–orbit interaction scales as $1/n^3$ (in eqn 2.56) and hence the splitting for $n = 3$ is $8/27 \simeq 0.3$ times that for $n = 2$.

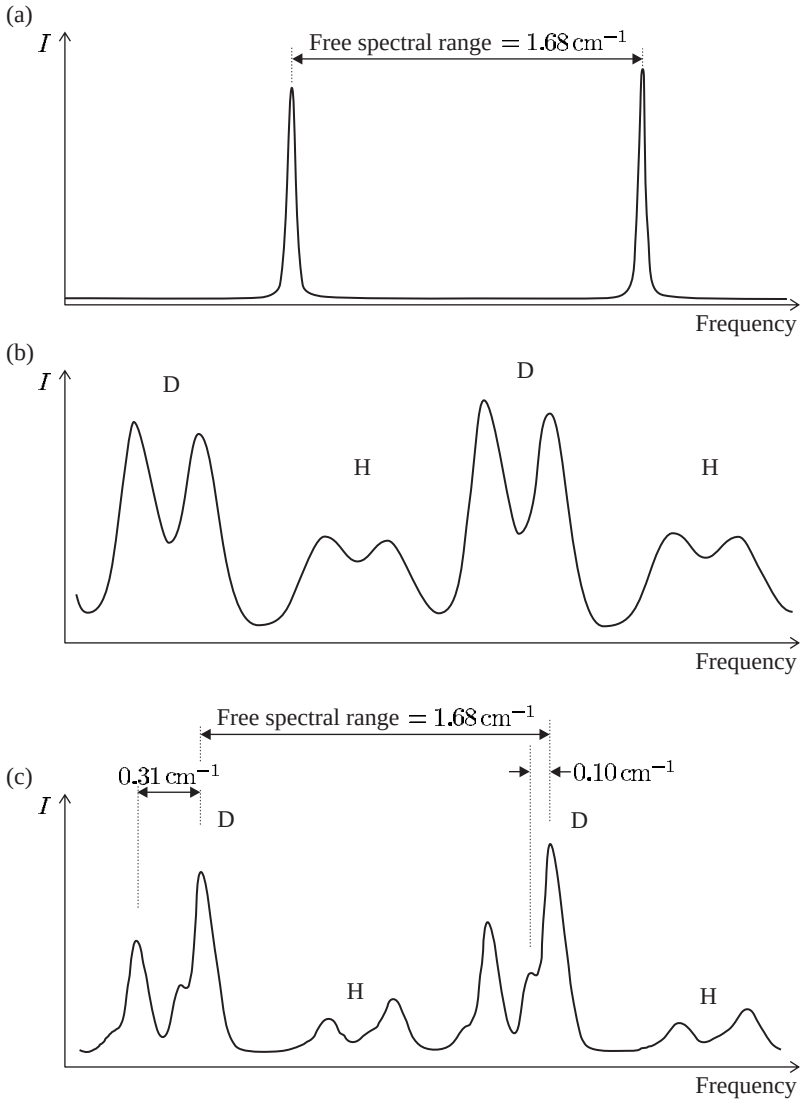

Fig. 8.6 Spectroscopy of the Balmer-α line, carried out with an apparatus similar to that in Fig. 1.7(a), has a resolution limited by the Doppler effect. (a) The transmission peaks of a pressure-scanned Fabry–Perot étalon obtained with a highly-monochromatic source (helium–neon laser). The spacing of the peaks equals the free-spectral range of the étalon given by FSR $= 1/2l = 1.68\,\mathrm{cm}^{-1}$, where l is the distance between the two highly-reflecting mirrors. The ratio of the FSR to the width of the peaks (FWHM) equals the finesse of the étalon, which is about 40 in this case. (The difference in height of the two peaks in this trace of real data arises from changes in laser intensity over time.) In all the traces, (a) to (c), the étalon was scanned over two free-spectral ranges. (b) The spectrum from a discharge of hydrogen, H, and deuterium, D, at room temperature. For each isotope, the two components have a separation approximately equal to the interval between the fine-structure levels with $n = 2$. This splitting is slightly larger than the Doppler width for hydrogen. The isotope shift between the hydrogen and deuterium lines is about 2.5 times larger than the free-spectral range, so that adjacent peaks for H and D come from different orders of the étalon. (The étalon length has been carefully chosen to avoid overlap whilst giving high resolution.) (c) The spectrum of hydrogen and deuterium cooled to around 100 K by immersing the discharge tube in liquid nitrogen. (The relative intensities change with discharge conditions.) The fine structure of the 3p configuration is not quite resolved, even for deuterium, but leads to observable shoulders on the left of each peak—the relevant energy levels are shown in Fig. 8.7. Courtesy of Dr John H. Sanders, Physics department, University of Oxford.

atomic hydrogen and part of the spectrum in Fig. 8.6(b) is shown for comparison.[23] The saturated absorption technique gives clearly resolved peaks from the 2a and 2b transitions with a separation equal to the Lamb shift—the QED contributions shift the energy of the 2s $^2\mathrm{S}_{1/2}$ level upwards relative to 2p $^2\mathrm{P}_{1/2}$. Lamb and Retherford had measured this shift by a radio-frequency method using a metastable beam of hydrogen

[23] The first saturated absorption spectrum of hydrogen was obtained by Professor Theodor Hänsch and co-workers at Stanford University (around 1972). In those pioneering experiments the width of the observed peaks was limited by the bandwidth of the pulsed lasers used. Continuous-wave lasers have lower bandwidth.

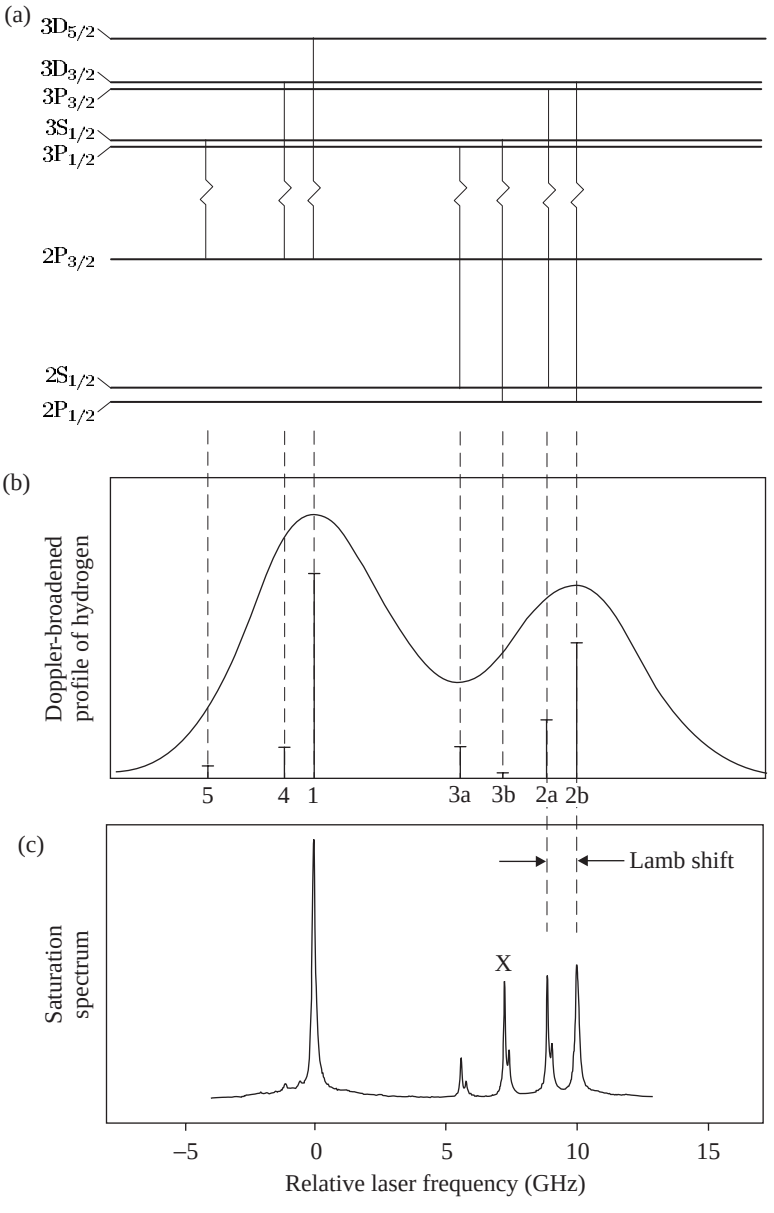

Fig. 8.7 Spectroscopy of the Balmer-α transition. (a) The levels with principal quantum numbers $n = 2$ and $n = 3$ and the transitions between them. Relativistic quantum mechanics (the Dirac equation) predicts that energies depend only on n and j, leading to the five transitions labelled 1 to 5 in order of decreasing strength (proportional to the square of the matrix element). In reality, some of these levels are not degenerate because of QED effects, e.g. the Lamb shift between 2s $^2S_{1/2}$ and 2p $^2P_{1/2}$ that gives two components in transitions 2 and 3. Thus there are seven optical transitions (that were listed in Section 2.3.5). (The allowed transition between the 2s $^2S_{1/2}$ and 2p $^2P_{1/2}$ levels, and other radio-frequency transitions are not marked.) (b) The Doppler-broadened profile of the Balmer-α line in a room-temperature discharge containing atomic hydrogen shows only two clear components separated by about 10 GHz (slightly less than the fine-structure splitting of the 2p configuration—see the caption of Fig. 8.6). (c) The saturated absorption spectrum obtained with a continuous-wave laser. The Lamb shift between the 2a and 2b components is clearly resolved. The 2s $^2S_{1/2}$ level has a hyperfine splitting of 178 MHz and this leads to the double-peaked profile of 2a, 3a and the cross-over resonance X midway between them. (In addition to their relative positions, further evidence that peak X is the cross-over resonance between 2a and 3a comes from their similar line shape, which strongly indicates that they share a common level; the weak transition 3b is obscured.) Transition 4 is also seen on the far left and the cross-over resonance between 4 and 1 is just visible as a small bump on the base of peak 1. The scale gives the laser frequency relative to an arbitrary point (transition 1). Data shown in (c) was obtained by Dr John R. Brandenberger and the author.

(atoms in 2s $^2S_{1/2}$ level) but it was not resolved by optical techniques before the invention of Doppler-free laser spectroscopy.

8.4 Two-photon spectroscopy

Two-photon spectroscopy uses two counter-propagating laser beams, as shown in Fig. 8.8. This arrangement has a superficial similarity to saturated absorption spectroscopy experiments (Fig. 8.4) but these two Doppler-free techniques differ fundamentally in principle. In two-photon spectroscopy the simultaneous absorption of two photons drives the atomic transition. If the atom absorbs one photon from each of the counter-propagating beams then the Doppler shifts cancel in the rest frame of the atom (Fig. 8.9(a)):

$$\omega\left(1+\frac{v}{c}\right)+\omega\left(1-\frac{v}{c}\right)=2\omega\,. \tag{8.20}$$

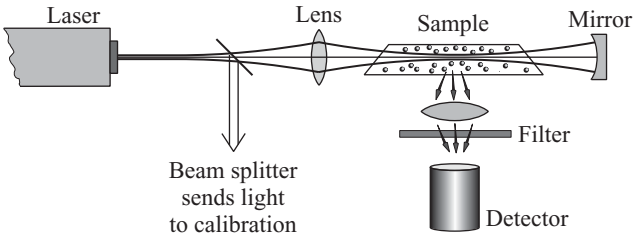

Fig. 8.8 A two-photon spectroscopy experiment. The lens focuses light from the tunable laser into the sample and a curved mirror reflects this beam back on itself to give two counter-propagating beams that overlap in the sample. For this example, the photons spontaneously emitted after a two-photon absorption have different wavelengths from the laser radiation and pass through a filter that blocks scattered laser light. Usually, only one of the wavelengths corresponding to the allowed transitions at frequencies ω_{1i} or ω_{i2} (in the cascade shown in Fig. 8.9(a)) reaches the detector (a photomultiplier or photodiode). The beam splitter picks off some laser light to allow measurement of its frequency by the methods discussed in Section 8.5.

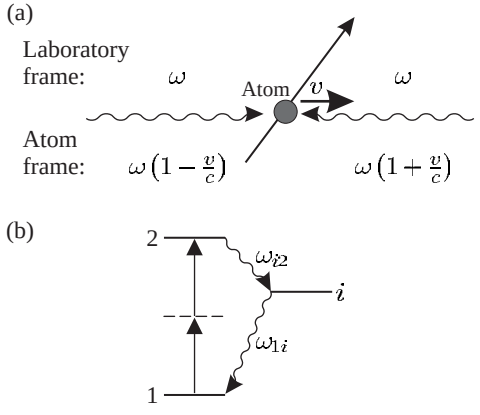

Fig. 8.9 (a) The atom has a component of velocity v along the axis of the laser beams (the light has frequency ω). The atoms sees an equal and opposite Doppler shift for each beam. So these shifts cancel out in the sum of the frequencies of the two counter-propagating photons absorbed by the atom (eqn 8.20). The sum of the frequencies does not depend on v so resonance occurs for all atoms when $2\omega = \omega_{12}$. (b) A two-photon transition between levels 1 and 2. The atom decays in two steps that each emit a single photon with frequencies ω_{i2} and ω_{1i}.

When twice the laser frequency ω equals the atomic resonance frequency $2\omega = \omega_{12}$ all the atoms can absorb two photons; whereas in saturation spectroscopy the Doppler-free signal comes only from those atoms with zero velocity.

For the energy-level structure shown in Fig. 8.9(b) the atom decays in two steps that each emit a single photon (following the two-photon absorption). Some of these photons end up at the detector. A brief consideration of this cascade process illustrates the distinction between a two-photon process and two single-photon transitions. It would be possible to excite atoms from 1 to 2 using *two* laser beams with frequencies $\omega_{\mathrm{L}1} = \omega_{1i}$ and $\omega_{\mathrm{L}2} = \omega_{i2}$ resonant with the two electric dipole transitions, but this two-step excitation has a completely different nature to the direct two-photon transition. The transfer of population via the intermediate level i occurs at the rate determined by the rates of the two individual steps, whereas the two-photon transition has a virtual intermediate level with no transitory population in i. (Equation 8.20 shows that to get a Doppler-free signal the two counter-propagating beams must have the same frequency.) This distinction between single- and two-photon transitions shows up clearly in the theory of these processes (see Section E.2 of Appendix E) and it is worthwhile to summarise some of the results here. Time-dependent perturbation theory gives the rate of transitions to the upper level induced by an oscillating electric field $\mathbf{E}_0 \cos \omega t$. The calculation of the rate of two-photon transitions requires second-order time-dependent perturbation theory. Resonant enhancement of the second-order process occurs when $2\omega = \omega_{12}$ but this still gives a rate which is small compared to an allowed single-photon transition. Therefore, to see any second-order effects, the first-order terms must be far off resonance; the frequency detuning from the intermediate level $\omega - \omega_{1i}$ must remain large (of the same order of magnitude as ω_{1i} itself, as drawn in the Fig. 8.9(b)). Two-photon absorption has many similarities with stimulated Raman scattering—a process of simultaneous absorption and stimulated emission of two photons via a virtual intermediate level, as shown in Fig. 8.10 (see Appendix E).

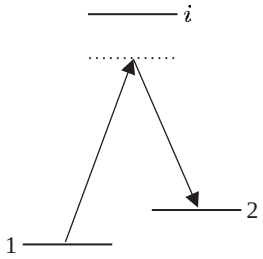

Fig. 8.10 A stimulated Raman transition between levels 1 and 2, via a virtual level. Level i is not resonantly excited in this coherent process.

Finally, although the difference between two sequential electric dipole transitions (E1) and a two-photon transition has been strongly emphasised above, these processes do link the same levels. So from the E1 selection rules ($\Delta l = \pm 1$ between levels of opposite parity) we deduce the two-photon selection rules: $\Delta l = 0, \pm 2$ and no change of parity, e.g. s–s or s–d transitions.

Two-photon spectroscopy was first demonstrated on the 3s–4d transition of atomic sodium which has a line width dominated by the natural width of the upper level. The 1s–2s transition in atomic hydrogen has an extremely narrow two-photon resonance, and the line width observed in experiments arises from the various broadening mechanisms that we study in the next section.

Example 8.3 *Two-photon spectroscopy of the* 1s–2s *transition in atomic hydrogen*

The 1s–2s two-photon transition in atomic hydrogen has an intrinsic natural width of only 1 Hz because the 2s configuration is metastable. An atom in the 2s energy level has a lifetime of 1/8 s, in the absence of any external perturbations, since there are no p configurations of significantly lower energy (see Fig. 2.2).[24] In contrast, the 2p configuration has a lifetime of only 1.6 ns because of the strong Lyman-α transition to the ground state (with a wavelength of 121.5 nm in the vacuum ultraviolet). This huge difference in lifetimes of the levels in $n = 2$ gives an indication of the relative strengths of single- and two-photon transitions. The 1s–2s transition has an intrinsic quality factor of $Q = 10^{15}$, calculated from the transition frequency $\frac{3}{4}cR_\infty$ divided by its natural width. To excite this two-photon transition the experiments required ultraviolet radiation at wavelength $\lambda = 243\,\text{nm}$.[25]

Figure 8.11 shows a Doppler-free spectrum of the 1s–2s transition. A resolution of 1 part in 10^{15} has not yet been achieved because the various mechanisms listed below limit the experimental line width.

(a) *Transit time* Two-photon absorption is a nonlinear process[26] with a rate proportional to the square of the laser beam intensity, I^2 (see Appendix E). Thus to give a high signal experimenters focus the counter-propagating beams down to a small size in the sample, as indicated in Fig. 8.8. For a beam diameter of $d = 0.5\,\text{mm}$ transit-time broadening gives a contribution to the line width of

$$\Delta f_{\text{tt}} = \frac{\Delta\omega_{\text{tt}}}{2\pi} \simeq \frac{u}{d} = \frac{2200\,\text{m s}^{-1}}{5 \times 10^{-4}\,\text{m}} = 4\,\text{MHz}\,, \qquad (8.21)$$

where u is a typical velocity for hydrogen atoms (see eqn 8.7).

(b) *Collision broadening (also called pressure broadening)* Collisions with other atoms, or molecules, in the gas perturb the atom (interacting with the radiation) and lead to a broadening and frequency shift of the observed spectral lines. This homogeneous broadening mechanism causes an increase in the line width that depends on the collision rate $1/\tau_{\text{coll}}$, where τ_{coll} is the average time between collisions. In a simple treatment, the homogeneous width of a transition whose natural width is Γ becomes $\Delta\omega_{\text{homog}} = \Gamma + 2/\tau_{\text{coll}} = \Gamma + 2N\sigma\overline{v}$, where σ is the collision cross-section and $\overline{v}$ is the mean relative velocity, as described by Corney (2000)—see also Loudon (2000) or Brooker (2003). The number density of the perturbing species N is proportional to the pressure. For the 1s–2s transition frequency the pressure broadening was measured to be 30 GHz/bar for hydrogen atoms in a gas that is mostly hydrogen molecules (H_2), and this gives a major contribution to the line width of the signal shown in Fig. 8.11 of about 8 MHz (at the frequency of the ultraviolet radiation near 243 nm).[27] Some further details are given in Exercise 8.7.

(c) *Laser bandwidth* The first two-photon experiments used pulsed lasers to give high intensities and the laser bandwidth limited the

[24] The microwave transition from the 2s $^2S_{1/2}$ level down to the 2p $^2P_{1/2}$ level has negligible spontaneous emission.

[25] Such short-wavelength radiation cannot be produced directly by tunable dye lasers, but requires frequency doubling of laser light at 486 nm by second-harmonic generation in a nonlinear crystal (a process that converts two photons into one of higher energy). Thus the frequency of the laser light (at 486 nm) is exactly one-quarter of the 1s–2s transition frequency (when both the factors of 2 for the frequency-doubling process and two-photon absorption are taken into account); thus the laser light (at 486 nm) has a frequency very close to that of the Balmer-β line ($n = 2$ to $n = 4$) because the energies are proportional to $1/n^2$ in hydrogen.

[26] In contrast, single-photon scattering *well below saturation* is a linear process proportional to the intensity I. Saturated absorption spectroscopy is a nonlinear process.

[27] Collisions shift the 1s–2s transition frequency by −9 GHz/bar and this pressure shift is more troublesome for precision measurements than the broadening of the line (see Boshier *et al.* 1989 and McIntyre *et al.* 1989).

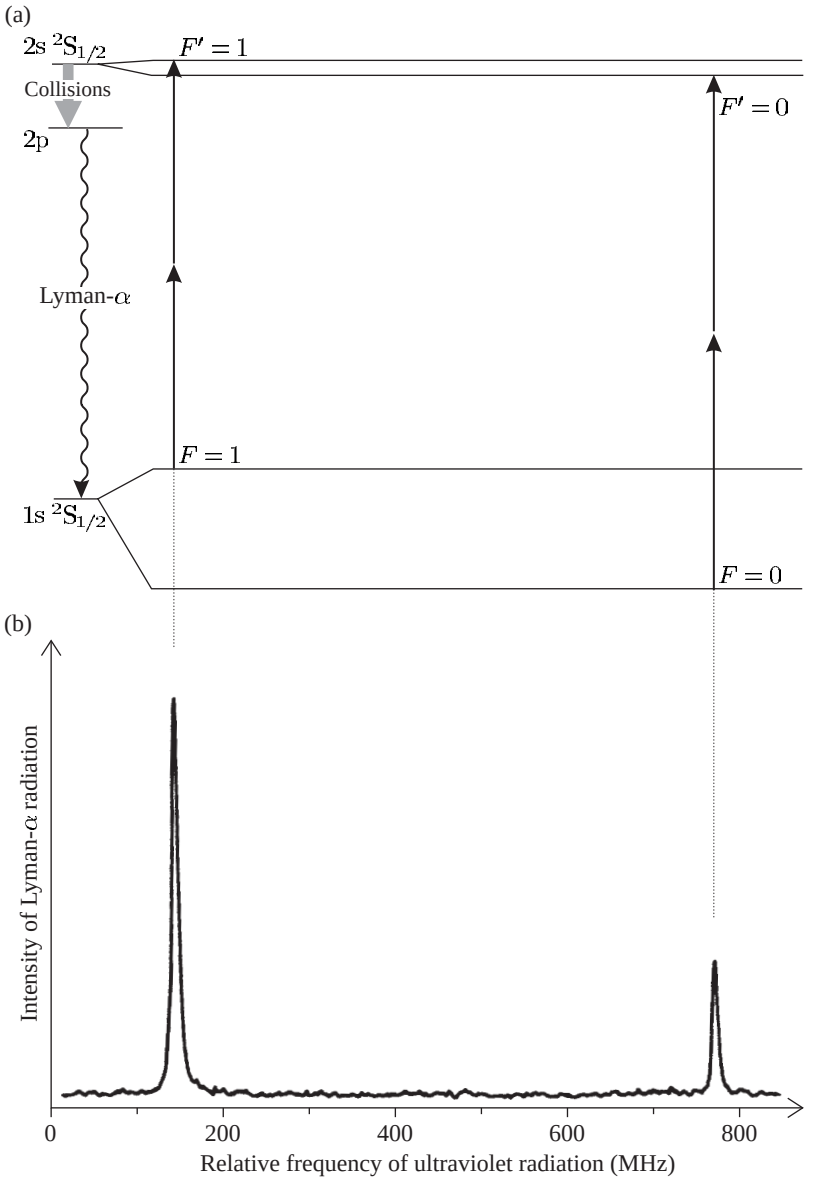

Fig. 8.11 (a) The hyperfine structure of the 1s and 2s configurations of hydrogen (not to scale). The two-photon transitions obey the selection rule $\Delta F = 0$. This allows the transitions $F = 0$ to $F' = 0$ and $F = 1$ to $F' = 1$. (b) A two-photon spectrum of the 1s–2s transition in atomic hydrogen. The recorded signal comes from photons emitted from the gas (following the two-photon excitation) that are detected by a photomultiplier, as shown in Fig. 8.8. This signal arises in a slightly different way to that shown in Fig. 8.9(b): the 2s configuration in hydrogen decays very slowly since it has no allowed transition to 1s but transfer from 2s to 2p occurs by collisions with atoms (or molecules) in the gas, and the 2p configuration decays rapidly by the emission of Lyman-α photons. The scale gives the (relative) frequency of the ultraviolet radiation used to excite the two-photon transition (Foot *et al.* 1985). Copyright 1985 by the American Physical Society.

resolution. A laser with a pulse of duration $\tau = 10\,\mathrm{ns}$ has a lower limit to its bandwidth of

$$\Delta f_\mathrm{L} \geqslant \frac{1}{\tau} \simeq 100\,\mathrm{MHz}\,. \tag{8.22}$$

This Fourier transform limit assumes a perfectly shaped pulse and in practice pulsed lasers typically have a bandwidth an order of magnitude greater. Commercial continuous-wave dye lasers have bandwidths of 1 MHz but researchers use sophisticated electronic servo-control systems to reduce this. The best ion trap experiments

use a laser system that generates ultraviolet radiation with a bandwidth of only a few Hz to give a resolution approaching 1 in 10^{15}.

(d) *Second-order Doppler effect* Two-photon spectroscopy eliminates the first-order Doppler effect but not the second-order term that corresponds to time dilation in special relativity, namely

$$\Delta f_{\mathrm{D2}} \sim \frac{u^2}{c^2} f_0 = 0.1\,\mathrm{MHz}\,. \tag{8.23}$$

For hydrogen $u/c = 7\times10^{-6}$ (see Section 8.1) and $f_0 = 2.5\times10^{15}\,\mathrm{Hz}$ for the 1s–2s transition.
Time dilation depends on the square of the atom's velocity and reduces the frequency of the emitted light seen by an observer in the laboratory, whichever direction the atom moves. This shifts the centre of the observed atomic line by an amount that depends on the velocity distribution of the atoms, and therefore causes uncertainty in precision measurements; it is worse than mechanisms that just broaden the line shape symmetrically about the atomic resonance frequency.

(e) *Light shift* The light shift, or a.c. Stark effect (Section 7.7), affects two-photon spectroscopy experiments because of the high intensities required to give reasonable transition rates. The shift of the centre of the observed line shape causes problems in precision experiments for the same reason as the second-order Doppler effect.[28]

[28] The light shift does not significantly affect 1s–2s experiments because only low-power ultraviolet beams are generated by nonlinear mixing.

Detailed calculations of all systematic effects on the 1s–2s transition frequency are given in Boshier *et al.* (1989) and McIntyre *et al.* (1989). Table 8.2 is a check-list of effects that may broaden the peaks in Doppler-free spectroscopy (and in some cases cause frequency shifts).

In his original experiment, Lamb, and his student Retherford, measured the shift between $2s\ ^2S_{1/2}$ and $2p\ ^2P_{1/2}$ directly with radio-frequency spectroscopy but the line width in their experiment was large

Table 8.2 Summary of broadening mechanisms in Doppler-free spectroscopy.

(i)	Natural broadening.
(ii)	Collisions (pressure broadening).
(iii)	Finite interaction time (transit-time broadening).
(iv)	Second-order Doppler effect.
(v)	Instrumental width—laser bandwidth.
(vi)	External fields—Zeeman and Stark effects.
(vii)	Residual Doppler broadening—if the beams are not exactly counter-propagating.
(viii)	Power broadening—related to saturation of the transition (in saturation spectroscopy).
(ix)	A.c. Stark effect—shift caused by the electric field of the light in two-photon spectroscopy.

because of the rapid decay of the 2p level (as mentioned at the beginning of this example). The 2p level has a natural width of 100 MHz—much larger than the line width in two-photon experiments. It is quite remarkable that the laser measurements of a transition frequency in the ultraviolet can exceed the precision of radio-frequency spectroscopy. Although the QED shifts represent only a very small part of the 1s–2s transition energy, the laser experiments determine these shifts accurately *if* the experimenters know the frequency of the laser. The following section describes methods used to measure the laser frequency and so calibrate the spectra.

8.5 Calibration in laser spectroscopy

Laser spectroscopy experiments use tunable lasers, i.e. laser systems whose frequency can be tuned over a wide range to find the atomic, or molecular, resonances. The early experiments used dye lasers in the visible region, e.g. the dye Rhodamine 6G gives the yellow light for experiments with sodium. The best dyes have a tunable range of over 50 nm and modern dyes exist that operate from the deep blue into the infra-red. However, the use of dyes in solution can be messy, and nowadays many experimenters prefer to use solid-state lasers that operate in the infra-red (Davis 1996); semiconductor diode lasers have a tuning range of about 10 nm, and the more general-purpose titanium-doped sapphire laser operates anywhere in the range 700–1000 nm. In comparison, the He–Ne laser only works within the Doppler profile of the neon transition; this has a Doppler width ~ 1 GHz at 633 nm corresponding to a wavelength range of only 0.001 nm. This fixed and well-defined wavelength can be used as a frequency reference (and similarly for other lasers operating on atomic transitions).

The method of calibrating the laser frequency depends on whether the experiment requires absolute or relative measurements.

8.5.1 Calibration of the relative frequency

Experiments that measure the separations of the components within the spectrum require an accurate frequency scale for the laser scan, e.g. in the measurement of the isotope shifts and hyperfine splittings shown in Fig. 6.12. To calibrate the laser scan, experimenters send part of the laser beam through a Fabry–Perot étalon and record the transmission, as shown in Fig. 8.12 (cf. Fig. 8.6(a)). The observed fringes have a spacing equal to the étalon's free-spectral range of $c/2l$ and l, the length of the cavity, can be measured accurately. In practice these experiments do need some method that gives the approximate wavelengths of the laser light, in order to find the atomic lines.

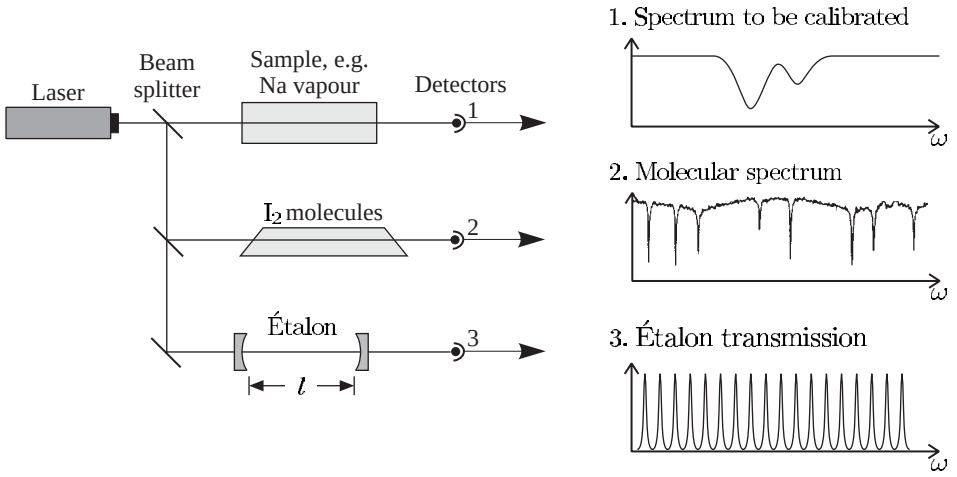

Fig. 8.12 Calibration of a laser experiment. Three signals are recorded: (1) the spectrum to be calibrated, e.g. the absorption of an atomic vapour; (2) a molecular spectrum, e.g. the absorption spectrum of iodine; and (3) the intensity transmitted through a Fabry–Perot étalon gives fringes with a frequency spacing equal to its free-spectral range $c/2l$, where l is the length of the étalon. These reference fringes provide the frequency scale. Molecular spectra have a 'forest' of lines so that there will be lines near any arbitrary wavelength and the individual lines can be identified by comparison with a known spectrum. These molecular lines give the absolute frequency. (The sodium cell is heated to give a vapour pressure sufficient for an absorption experiment.)

8.5.2 Absolute calibration

To determine the absolute frequency of a spectral line it is compared to a nearby line of known frequency (or wavelength)—the same principle as in the use of a calibration lamp to produce fiducial lines on a spectrum obtained from a conventional prism spectrograph (or diffraction grating). Laser spectroscopists often use iodine to provide the reference lines because its molecular spectrum has many lines in the visible region and an atlas of iodine wavelengths has been compiled for this purpose (Gerstenkorn *et al.* 1993). Molecules have many more transitions than atoms and this gives a high probability of finding a suitable line near any frequency of interest. Iodine has sufficient vapour pressure at room temperature to give measurable absorption in a simple glass cell as shown in Fig. 8.12. The figure uses the Doppler-broadened absorption in sodium as an example of the spectrum to be measured. The iodine lines have much narrower Doppler widths because of the heavy molecular mass (I_2 has molecular weight 254).

The calibration of Doppler-free spectra often requires narrower reference lines obtained by saturation spectroscopy on the iodine itself (see Corney 2000, Figs 13.13 and 13.14). The frequency of the 1s–2s transition in atomic hydrogen described in Example 8.3 has been measured relative to a line in the saturated absorption spectrum of tellurium,[29] as shown in Fig. 8.13. The experiment was calibrated by the following procedure. The saturation spectroscopy of Te_2 was carried out with blue light of wavelength 486 nm and angular frequency ω_L. Some of

[29] A heavy diatomic molecule like iodine, but Te_2 happens to have lines in the blue region whereas I_2 does not.

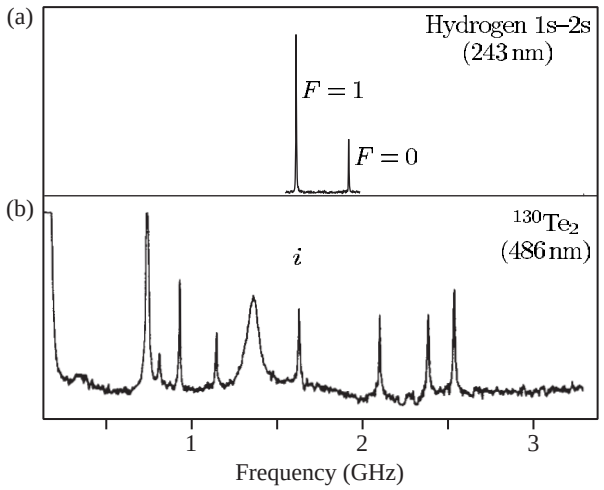

Fig. 8.13 (a) A two-photon spectrum of the 1s–2s transition in atomic hydrogen as in Fig. 8.11 but on a different scale. (b) The saturated absorption spectrum of molecular tellurium used for calibration. The absolute frequency of the line labelled i was determined with an uncertainty of 6×10^{-10} (by auxiliary measurements). Adapted from McIntyre *et al.* (1989). Copyright 1989 by the American Physical Society.

this blue light was passed through a nonlinear crystal where the process of second-harmonic generation produced some radiation of frequency $\omega = 2\omega_L$. The frequency of this ultraviolet radiation at 243 nm was compared with the radiation (with a very similar frequency) that excited the 1s–2s transition. Thus the two-photon resonance condition in eqn 8.20 is $\omega_{12} = 2\omega = 4\omega_L$. The 1s $^2S_{1/2}$ $F = 1$ to 2s $^2S_{1/2}$ $F = 1$ transition has almost exactly four times the frequency of the line i in the spectrum of Te_2, and the small frequency offset can be measured precisely.

This method of calibration in terms of known spectral lines begs the question of how to determine the frequencies of the reference lines themselves in the first place. The short answer is that experimenters rely on the national standards laboratories around the world to measure suitable reference lines and to establish internationally agreed frequency standards, e.g. the particular iodine line that coincides with the output of the He–Ne laser at 633 nm has been measured very accurately. A helium–neon laser with its frequency controlled to be equal to that of the iodine line provides a portable frequency standard, i.e. one calibrated by the standard laboratory and then carried to the experimental laboratory to provide a reference (see Corney 2000, Section 13.10). The national standards laboratories must calibrate the secondary frequency standards in terms of the primary standard of time provided by the caesium atom clock at a frequency of 9 GHz (as described in Chapter 6). Until recently, a frequency chain was required to relate an optical frequency to a microwave frequency standard. A frequency chain comprises many oscillators, such as microwave sources and lasers, whose frequencies are multiples of each other, as indicated in Fig. 8.14. To go from 9 GHz up to around 6×10^{14} Hz (corresponding to visible light) required many different oscillators as links in the chain. All these devices must operate simultaneously and have their frequencies electronically controlled relative to those of neighbouring oscillators this makes such high precision

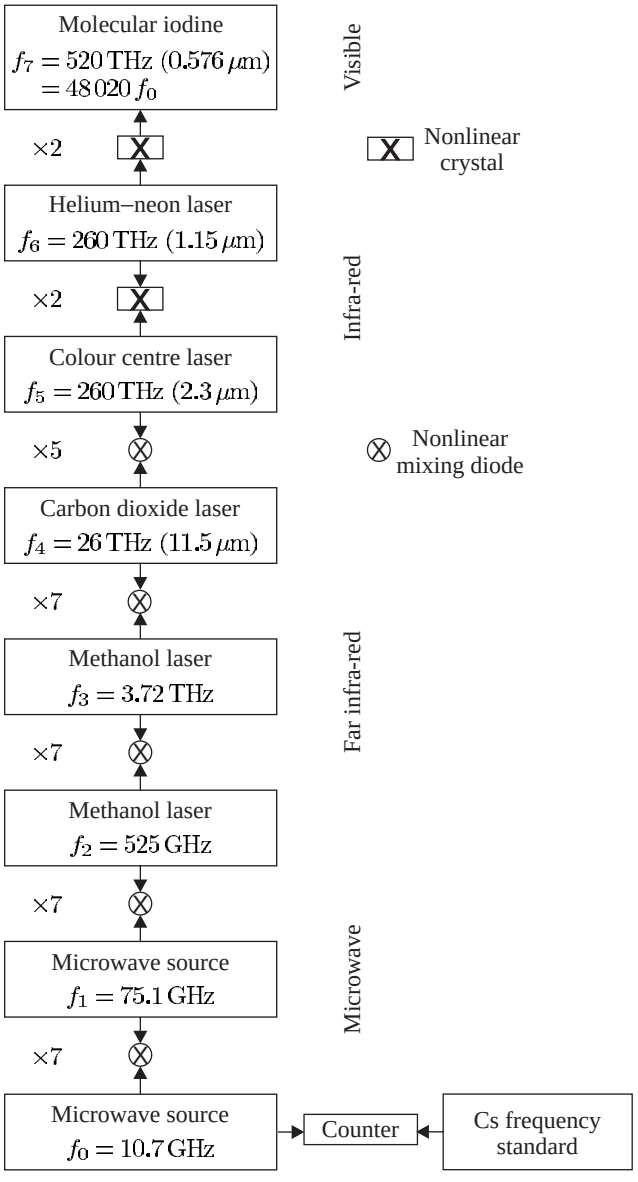

Fig. 8.14 A frequency chain. The frequency of a line in the visible spectrum of molecular iodine is measured by setting up a chain of oscillators. The frequency of each oscillator is compared to a multiple or sum of the frequencies of the other oscillators. At the bottom of the chain is a microwave source whose frequency is measured with reference to a caesium frequency standard (the primary time standard as described in Section 6.4.2). A diode mixer produces a high number of harmonics of the microwaves, so that the first few stages achieve multiplication by a factor of 7. Nonlinear crystals are used for mixing mid-infra-red and visible radiation. The scheme shown here is one of the least complicated but it still involves a large number of devices. When the whole chain is operating it determines the multiplication factor that relates the optical frequency to the caesium frequency standard at 9 GHz. After Jennings *et al.* (1979).

measurements are a major undertaking. Recently, a new method has been invented that supersedes cumbersome frequency chains and makes the measurement of optical frequencies more straightforward.

8.5.3 Optical frequency combs

Recently, a new method of measuring optical frequencies has been invented that has revolutionised optical metrology. The new method relies on the ability to generate frequency combs using laser techniques, i.e. laser radiation that contains a set of regularly-spaced frequencies, as

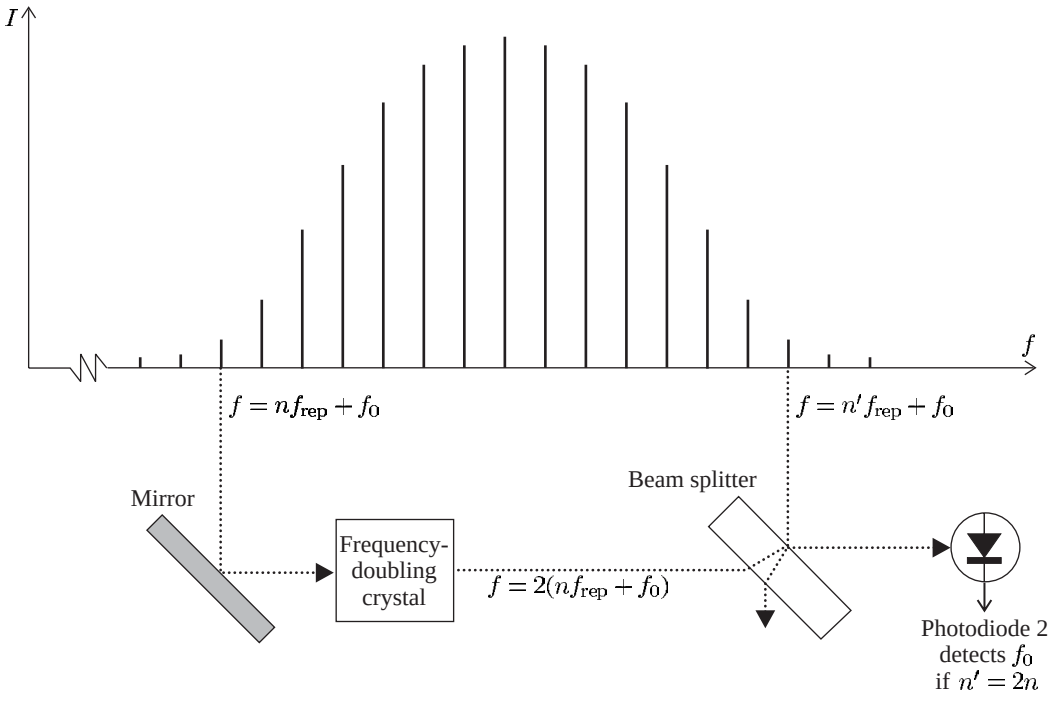

Fig. 8.15 A frequency comb produced by a femtosecond laser system (and an optical fibre)—in reality there are many more regularly-spaced modes than are shown here. The frequencies spread over an octave so that modes on the low- and high-frequency wings can be compared, using second-harmonic generation in a nonlinear crystal, to determine the frequency offset of the comb as in eqn 8.25.

illustrated in Fig. 8.15. The frequency comb contains the frequencies

$$f = f_0 + nf_{\text{rep}}\,, \tag{8.24}$$

where f_{rep} is the frequency interval and f_0 is an offset from zero that we shall assume is smaller than f_{rep} (for this choice n will be a large positive integer). A laser produces such a frequency spectrum; however, there is not room here for a detailed description of the laser physics of such systems, see Davis (1996) or Meschede (2004).[30] The frequency spectrum is related by a Fourier transform to a train of short pulses in the time domain; the time interval between pulses t_{rep} and the spacing in the frequency are related by $f_{\text{rep}} = 1/t_{\text{rep}}$.[31]

The frequency span of the comb, i.e. the width of the spectrum's envelope in Fig. 8.15, is inversely proportional to the duration of each individual pulse. Actually, in the historical development of pulsed lasers this was viewed the other way around—the objective was to create the shortest pulses possible and this requires the laser medium to have gain over a wide spectral region. The titanium-doped sapphire laser used in the frequency comb experiments created pulses with a duration less than 100 fs ($< 10^{-13}$ s, see Holzwarth *et al.* (2000)). Such femtosecond lasers have great technical importance, both for studying processes with

[30] A very short pulse of light propagates around the optical cavity of the laser formed by high-reflectivity mirrors. One of these mirrors is less reflective than the others so that it transmits a few per cent of the light. Each time the short pulse hits this output coupling mirror part of the pulse travels out of the cavity to give a steady train of short pulses that emerge from the laser with a time interval of t_{rep} between them. This time interval between pulses equals the round trip length of the laser cavity L divided by the speed of light: $t_{\text{rep}} = L/c$.

[31] This behaviour is closely analogous to the situation of light reflected from a diffraction grating, where the angular separation of the diffraction orders is inversely proportional to the spacing between the rulings, or slits for a transmission grating. For a detailed description of Fourier transforms and diffraction gratings see Brooker (2003).

very high time resolution and for creating pulses of extremely high peak intensity (by compressing a high-energy pulse into a very short time).

The frequency $f_{\rm rep}$ is measured by directing some of the laser light onto a photodiode (see Fig. 8.16). The femtosecond laser does not produce a sufficiently wide spread in frequencies for the specific scheme illustrated in Figs 8.15 and 8.16. This is obtained by sending the output of the femtosecond laser along a special highly-dispersive optical fibre, as indicated schematically in Fig. 8.16. The combination of the femtosecond laser and this special fibre produces radiation with the frequency spectrum in eqn 8.24, that spans a large spectral range, e.g. from 520 nm to 1170 nm in the work of Udem *et al.* (2001), equivalent to a frequency range of 300 THz. For $f_{\rm rep} = 1$ GHz this range of values corresponds to $n = 2.5$ to 6×10^6.

After the frequency comb has been generated, the next stage is to determine the offset f_0 by an ingenious method devised by Professor Theodor Hänsch and co-workers, namely a comparison, or self-referencing, of the frequency of lines from different parts of the frequency comb. This is achieved by sending the light (from the low-frequency wing of the comb) through a frequency-doubling crystal; in this nonlinear optical medium some radiation is generated at the second harmonic of the input frequency. The light emerging from the crystal has frequency components $2(n' f_{\rm rep} + f_0)$, where n' is an integer (the reason for introducing

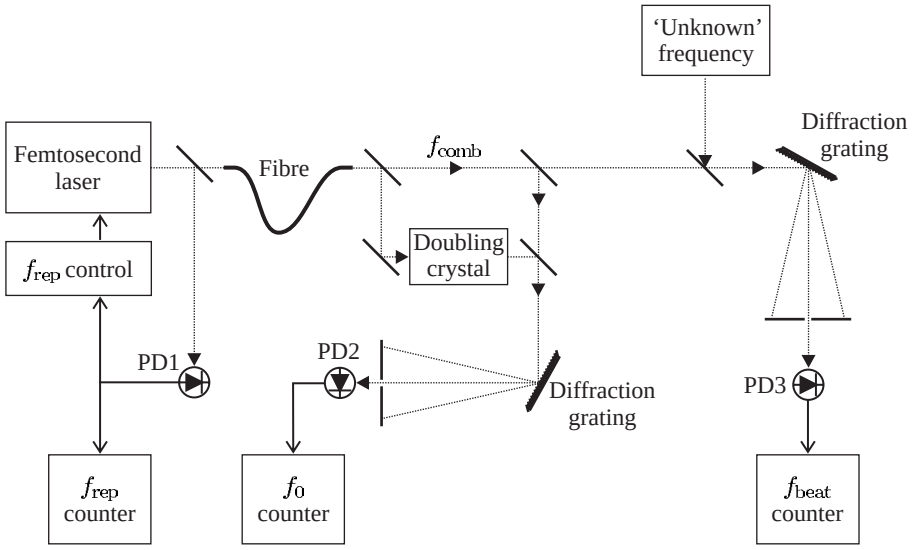

Fig. 8.16 The experimental arrangement for the measurement of an optical frequency using a frequency comb from a femtosecond laser. Photodiode 1 measures the frequency interval between the laser modes, $f_{\rm rep}$ in eqn 8.24, and $f_{\rm rep}$ is maintained constant by electronic feedback from the frequency counter to the laser (the laser cavity length is kept fixed by adjusting the position of a mirror with a piezoelectric actuator). Photodiode 2 measures the beat frequency between modes in the low- and high-frequency wings of the comb (see Fig. 8.15). Photodiode 3 measures the frequency difference between one mode of the comb and the unknown laser frequency as in eqn 8.26. The diffraction gratings spread out the light so that only the relevant part of the frequency comb falls onto the detector, as explained in the text. Figure courtesy of Dr Helen Margolis, National Physical Laboratory; after Margolis *et al.* (2003).

both n' and n will become apparent shortly). This radiation mixes with some of the original light, whose frequency is given by eqn 8.24, on a photodiode. The signal from this detector contains the frequencies

$$f = 2(n' f_{\rm rep} + f_0) - (n f_{\rm rep} + f_0) = (2n' - n) f_{\rm rep} + f_0 \,. \qquad (8.25)$$

For a frequency comb that spans an octave there are frequency components with $n = 2n'$, i.e. high-frequency lines that have twice the frequency of lines on the low-frequency wing. For these lines eqn 8.25 reduces to f_0, and in this way the frequency offset is measured.[32] In Fig. 8.16 the photodiodes 1 and 2 measure precisely the radio frequencies $f_{\rm rep}$ and f_0, respectively, and hence determine the frequency of each line in the comb (eqn 8.24).[33]

The light from the calibrated frequency comb is mixed with some of the output of the continuous-wave laser whose frequency $f_{\rm L}$ is to be measured, whilst the remaining light from this second laser is used for experiments, e.g. high-resolution spectroscopy of atoms or molecules. The third photodiode measures the beat frequency, which is equal to the difference between $f_{\rm L}$ and the nearest component of the frequency comb:[34]

$$f_{\rm beat} = |n'' f_{\rm rep} + f_0 - f_{\rm L}| \,. \qquad (8.26)$$

This beat frequency is measured by a radio-frequency counter.

The unknown laser frequency is determined in terms of the three measured frequencies as $f_{\rm L} = n'' f_{\rm rep} + f_0 \pm f_{\rm beat}$. It is assumed that $f_{\rm L}$ is known with an uncertainty less than $f_{\rm rep}$, so that the value of the integer n'' is determined, e.g. when $f_{\rm rep} = 1\,{\rm GHz}$ (as above) and $f_{\rm L} \simeq 5 \times 10^{14}$ (corresponding to a visible wavelength) it is necessary to know $f_{\rm L}$ to a precision greater than 2 parts in 10^6, which is readily achieved by other methods. The measurement of radio frequencies can be carried out extremely accurately and this frequency comb method has been used to determine the absolute frequency of very narrow transitions in atoms and ions,[35] e.g. Ca, Hg^+, Sr^+ and Yb^+—see Udem *et al.* (2001), Blythe *et al.* (2003) and Margolis *et al.* (2003). These experiments were limited by systematic effects such as perturbing electric and magnetic fields, that can be improved by further work. The uniformity of the spacing of the lines in the frequency comb has been verified to at least a few parts in 10^{16}, and in the future it is anticipated that uncertainties in measurements of frequency of very narrow transitions in ions, trapped using the techniques described in Chapter 12, can be reduced to a few parts in 10^{18}. At such an incredible level of precision new physical effects may show up. For example, it has been suggested that fundamental 'constants' such as the fine-structure constant α may vary slowly on astrophysical time-scales, and this would lead to changes in atomic transition frequencies with time. If such variations do indeed occur, then an inter-comparison of frequency standards that depend on different powers of α over many years is potentially a way to observe them.

[32] Other schemes have been demonstrated, e.g. choosing $2n = 3n'$ so that the frequency comb does not have to be so wide and can be generated directly from a laser (eliminating the optical fibre in Fig. 8.16).

[33] A diffraction grating is used to spread out the light at different wavelengths so that only the high-frequency part of the spectral region where $n = 2n'$ falls onto the detector. Light at other wavelengths produces unwanted background intensity that does not contribute to the signal.

[34] The beat frequencies with other components fall outside the bandwidth of the detector.

[35] This method has also been used to calibrate a selection of molecular iodine lines that can be used as secondary frequency standards, as described in the previous section (Holzwarth *et al.* 2000).

Further reading

This chapter has focused on just a few examples of Doppler-free laser spectroscopy and calibration to illustrate the important principles. Such measurements of the transition frequencies in atomic hydrogen give a precise value for the Rydberg constant and the QED shift. More details of the saturated absorption and two-photon methods are given in specialised books on laser spectroscopy by Letokhov and Chebotaev (1977), Demtröder (1996), Corney (2000) and Meschede (2004)—the last of these gives details of recent experiments on the 1s–2s transition in atomic hydrogen. Nowadays, laser spectroscopy is very widely used in more complex situations, e.g. liquids and solids.

The monograph by Series (1988) on the spectrum of atomic hydrogen gives a comprehensive description that includes Lamb and Retherford's historic experiment and later refinements of the radio-frequency techniques, as well as laser spectroscopy. The series of proceedings of the biennial International Conference on Laser Spectroscopy (published by Springer-Verlag) gives an overview of the current state of the art and current applications. The measurement of the absolute frequency of light using optical frequency combs is a relatively new technique but already it has had an important impact on optical frequency metrology (Udem *et al.* 2002).

Exercises

(8.1) *Doppler widths*
Calculate the Doppler width of a spectral line with a wavelength of 589 nm for (a) sodium vapour at 1000 K, and (b) a vapour of molecular iodine at room temperature.

(8.2) *Doppler broadening*
The two fine-structure components of the 2s–2p transition in a lithium atom have wavelengths of 670.961 nm and 670.976 nm (in a vacuum). Estimate the Doppler broadening of this line in a room-temperature vapour and comment on the feasibility of observing the weak-field Zeeman effect in lithium.

(8.3) *Crossed-beam technique*
The figure shows the fluorescent signal obtained from a crossed-beam experiment like that presented in Fig. 8.2. Radiation of wavelength 243 nm excited a single-photon transition in strontium atoms from an oven at a temperature of 900 K. Each peak is labelled with the relative atomic mass of the isotope. The frequency scale was calibrated by sending some light through a Fabry–Perot étalon (cf. Fig. 8.12) to produce marker fringes with a frequency spacing of 75 MHz.

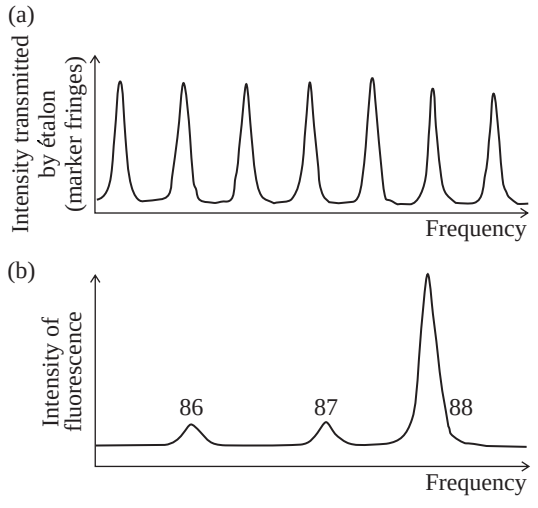

Determine the line width of the peaks and the frequency shift between the even isotopes from the scan. The line width arises from residual Doppler broadening. Calculate the collimation angle of the atomic beam.

Comment. This line has a normal mass shift of 180 MHz between the two even isotopes. There are smaller contributions to the isotope shift from the specific mass and volume effects.

(8.4) *Hyperfine structure in laser spectroscopy*
What is the physical origin of the interaction that leads to hyperfine structure in atoms?
Show that hyperfine splittings obey an interval rule which can be expressed as

$$\Delta E_{F,F-1} = A_{nlj} F \,,$$

i.e. the splitting of two sub-levels is proportional to the total angular momentum quantum number F of the sub-level with the larger F.
The naturally-occurring isotope of caesium (^{133}Cs) has a nuclear spin of $I = 7/2$. Draw a diagram showing the hyperfine sub-levels, labelled by the appropriate quantum number(s), that arise from the 6 ^{2}S$_{1/2}$ and 6 ^{2}P$_{3/2}$ levels in caesium, and the allowed electric dipole transitions between them.
Explain the principle of Doppler-free saturation spectroscopy.
The figure shows the saturated absorption spectrum obtained from the 6 ^{2}S$_{1/2}$–6 ^{2}P$_{3/2}$ transition in a vapour of atomic caesium, including the cross-over resonances which occur midway between *all* pairs of transitions whose frequency separation is less than the Doppler width. The relative positions of the saturated absorption peaks within each group are given below in MHz.

A	B	C	D	E	F
0	100.7	201.5	226.5	327.2	452.9

a	b	c	d	e	f
0	75.8	151.5	176.5	252.2	353.0

Using these data and the information in the diagram:

(a) determine the extent to which the interval rule is obeyed in this case and deduce the hyperfine parameter A_{nlj} for the 6 ^{2}S$_{1/2}$ and 6 ^{2}P$_{3/2}$ levels;

(b) estimate the temperature of the caesium vapour. (The wavelength of the transition is 852 nm.)

(8.5) *Hyperfine structure in laser spectroscopy*
The energy separation between the two hyperfine levels in the ns configurations of hydrogen is given by eqn 6.10, and for $n = 1$ this corresponds to a hyperfine transition frequency of $\Delta f_{\mathrm{HFS}}(1\mathrm{s}) = 1.4\,\mathrm{GHz}$.

(a) Determine the separation of the hyperfine sublevels in the 2s ^{2}S$_{1/2}$ level of hydrogen, and compare your answer to the value in the caption of Fig. 8.7.

(b) Show that the peaks presented in Fig. 8.11 have an expected separation of $\frac{7}{16}\Delta f_{\mathrm{HFS}}(1\mathrm{s})$. Compare the expected value with that in the figure (e.g. by measurement with a ruler and using the frequency scale given).

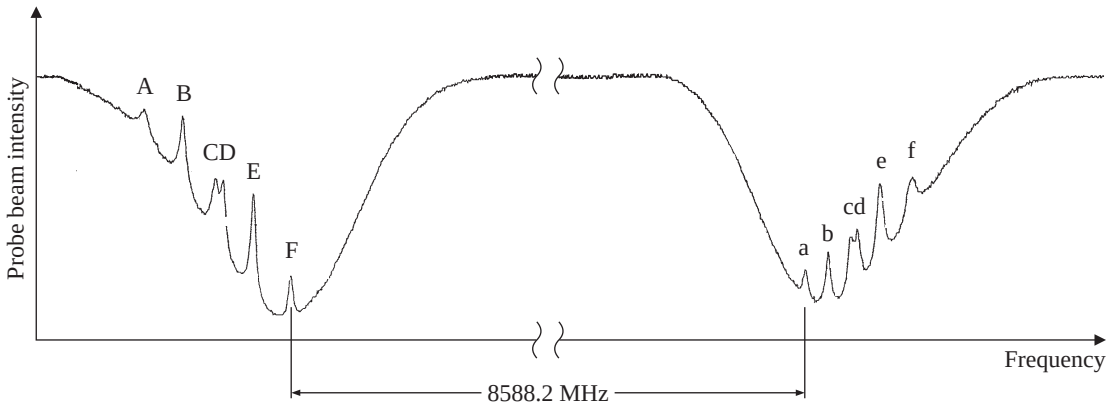

(8.6) *Two-photon experiment*

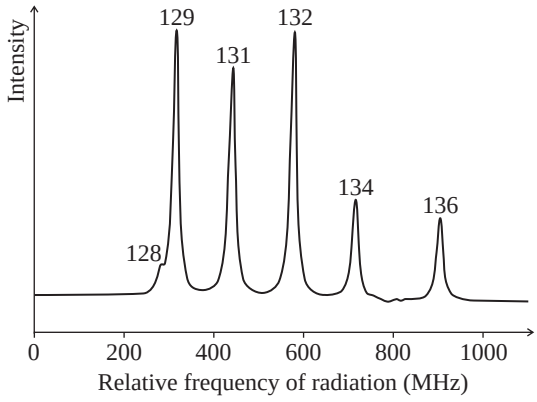

The above experimental scan comes from a two-photon experiment like that shown in Fig. 8.8. The transition from the $5p^6\ {}^1S_0$ ground level of xenon to a $J = 0$ level of the $5p^5 6p$ configuration was excited by ultraviolet radiation with a wavelength of 249 nm and the scale gives the (relative) frequency of this radiation. This $J = 0$ to $J' = 0$ transition has no hyperfine structure and the peak for each isotope is labelled with its relative atomic mass. The xenon gas was at room temperature and a pressure of 0.3 mbar. Light from a blue dye laser with a frequency jitter of 1 MHz was frequency-doubled to generate the ultraviolet radiation and the counter-propagating beams of this radiation had a radius of 0.1 mm in the interaction region.

Estimate the contributions to the line width from (a) the transit time, (b) pressure broadening, (c) the instrumental width, and (d) the Doppler effect.

(8.7) *Collision broadening of a two-photon transition*

The signal shown in Fig. 8.11 has a line width (FWHM) of about 10 MHz. From the data given in Example 8.3 determine the maximum pressure of hydrogen which could have been used in that experiment.

Later experiments[36] measured the pressure broadening of the 1s–2s transition frequency to be 20 GHz/bar for hydrogen atoms in a gas that is mostly helium atoms. Estimate the cross-section for collisions between metastable hydrogen and helium atoms. Comment on the size of this cross-section in relation to the size of atoms.

(8.8) *Convolution of Lorentzian line shapes*

A simple quantitative model of saturated absorption spectroscopy is given in Appendix D and this exercise examines some of the mathematical details.

(a) The convolution of two Lorentzian functions of equal width can be found using

$$\int_{-\infty}^{\infty} \frac{1}{1+(2y-x)^2}\,\frac{1}{1+x^2}\,\mathrm{d}x = \frac{1}{2}\,\frac{\pi}{1+y^2}\,. \tag{8.27}$$

Calculate the integral in eqn D.6. Hence prove eqn D.7.

(b) The convolution of two Lorentzian functions of unequal widths is

$$\int_{-\infty}^{\infty} \frac{1}{a^2+(y+x)^2}\,\frac{1}{b^2+(y-x)^2}\,\mathrm{d}x = \left(\frac{a+b}{ab}\right)\frac{\pi}{(2y)^2+(a+b)^2}\,. \tag{8.28}$$

Use this to show that taking into account the power broadening of the hole burnt in populations by the pump beam leads to a predicted line width in saturation spectroscopy of

$$\Gamma' = \frac{1}{2}\Gamma\left(1+\sqrt{1+\frac{I}{I_{\mathrm{sat}}}}\right).$$

Comment. The proof of eqns 8.27 and 8.28 requires the residue theorem for complex path integrals.

Web site:

`http://www.physics.ox.ac.uk/users/foot`

This site has answers to some of the exercises, corrections and other supplementary information.

[36] See Boshier *et al.* (1989) and McIntyre *et al.* (1989).

9 Laser cooling and trapping

In previous chapters we have seen how laser spectroscopy gives Doppler-free spectra and also how other older techniques of radio-frequency and microwave spectroscopy can resolve small splittings, e.g. hyperfine structure. These methods just observe the atoms as they go past,[1] but this chapter describes the experimental techniques that use the force exerted by laser light to slow the atomic motion and manipulate atoms. These techniques have become extremely important in atomic physics and have many applications, e.g. they have greatly improved the stability of the caesium atomic clocks that are used as primary standards of time around the world. We shall look at the forces that laser light exerts on an atom in some detail since this aspect contains most of the atomic physics. In many of the cases studied in this chapter, the atom's motion follows straightforwardly from Newton's laws once the force is known—an atom behaves like a classical particle, localised at a particular point in space, when the atomic wavepacket has a spread which is small compared to the distance over which the potential energy varies.[2]

The first laser cooling experiments were carried out on ions that were trapped by electric fields and then cooled by laser radiation. In contrast, it is difficult to confine atoms at room temperature, or above, because of the smaller electromagnetic forces on neutral particles. Therefore the pioneering experiments used light forces to slow atoms in an atomic beam and then confined the cold atoms with a magnetic field. The great success of laser cooling led to the award of the 1997 Nobel prize in physics to Steven Chu, Claude Cohen-Tannoudji and William Phillips. To describe the development of the subject we consider their contributions in the following order. We start from an explanation of the light force on atoms in terms of the scattering of photons. The research group of Phillips used this force to slow an atomic beam (Section 9.2). Chu and co-workers then demonstrated the method known as the optical molasses technique, that cools the motion of atoms in all three dimensions to give a very cold atomic vapour (Section 9.3). This led directly to the development of the so-called magneto-optical trap (Section 9.4) used in the majority of atom-trapping experiments today.

The interaction of the atoms with the light field turned out to be much more subtle than first supposed, and experiments showed that the optical molasses technique produced even lower temperatures than predicted. Cohen-Tannoudji and Jean Dalibard explained this behaviour by a new mechanism called Sisyphus cooling.[3] This mechanism is described towards the end of the chapter (Section 9.7) since it does not

[1] The inhomogeneous magnetic field deflects the atoms in the Stern–Gerlach experiment but has a negligible effect on the speed.

[2] This condition does not hold true for cold atoms moving through a standing wave of light where the intensity varies significantly over short distances (comparable with the optical wavelength, see Section 9.7).

[3] Chu and co-workers also developed a physically equivalent description.